Geometrical frustration in nonlinear photonic lattices

E. Arévalo and L. Morales-Molina
Facultad de Física, Pontificia Universidad Católica de Chile, Casilla 306, Santiago, Chile

(Received 20 April 2018; published 31 August 2018)

Geometrical frustration in either classical or quantum lattice systems is a phenomenon in which the impossibility of satisfying simultaneously all constraints of the system Hamiltonian leads to complex structures with degeneracy of the ground state. We show that geometrical frustration can be observed in a simple setup consisting of classical light propagating along a regular array of evanescently coupled photonic nonlinear waveguides arranged in a honeycomb geometry. Here, geometrical frustration emerges as competition between the number of waveguides and the need to satisfy the stationary constraints of the system. The phenomenology that exhibits these photonic arrays mimics the behavior observed in graphene-related spin lattices. Our results show that two-dimensional arrays of coupled photonic waveguides can be used as a proxy to study geometry frustration in diverse lattice systems.

DOI: 10.1103/PhysRevA.98.023864

I. INTRODUCTION

Geometrical frustration (GF) has been an issue of great interest in magnetic materials displaying magnetic ordering. This is mainly because of the fascinating nontrivial magnetic structures [1–3] that emerge and play a role in phenomena such as quantum Hall effect [4–6], superconductivity [7], quasiparticles resembling monopoles [8,9], etc. GF has been also synthetically engineered with the help of materials exhibiting magnetic properties such as ultracold atoms [10–12], Josephson junctions [13,14], single-domain ferromagnetic islands [15], magnetically doped colloidal crystals [16,17], synthetic spin lattices [18], among others.

Usually the degeneracy of the ground state in classical and quantum systems arises from the same geometry, so GF signatures may be observed in different physical platforms [19,20]. For instance, it has been shown that GF signatures can arise from complex networks [21,22] or from quantum circuits with nonclassical light [19]. However, despite the generality of the phenomenon, little is known about GF arising from classical light waves in a guided medium. In this regard, recently a lack of long-range laser phase ordering arising from thousands of coupled lasers has been associated with signatures of large-scale GF, similar to that observed in magnetic systems [20]. However, beyond this proposal, observations of GF signatures with classical light have been elusive in optical systems in general. In particular, to the best of our knowledge, no known study on GF emerging from an optically guided medium exists, so far.

Relevant examples of a guided medium are the arrays of evanescently coupled photonic waveguides [23], or in short, photonic waveguided arrays (PWA). Classical light propagating in PWA has been used to mimic diverse geometrical phenomena observed in condensed matter physics as, for instance, Bloch-Zener oscillations [24–26], Klein tunneling [27], transport and Anderson localization [28], synthetic magnetic fields [29], broken time-reversal symmetry [30], topological transitions [31], Floquet topological insulators [32], or four-dimensional quantum physics [33]. Nevertheless, it remains as an open question whether classical light propagating in PWA can be used as a platform for studying GF.

To tackle this question, we consider a two-dimensional (2D) nonlinear PWA with a pristine honeycomb geometry. We choose this array geometry not only for the great scientific and technological interest in graphene [34,35] and other honeycomb structures [32,36] but also for the signatures of GF emergence observed in honeycomb spin lattices [1,2,11]. Our final goal is to obtain an insight into the relation between GF emergence in guided media, nonlinearity, and transport phenomena in honeycomb PWA.

In honeycomb spin lattices, GF has been predicted for half-filled lattice graphene nanoflakes at zero energy [1]. It suggests that GF, in honeycomb systems, can arise at the Dirac points, i.e., isolated points where the upper and lower parts of the lowest quasienergy band touch each other [37–39]. Due to the double conical geometry of the band structure near the Dirac points, very high mobility has been predicted and observed in graphene and other honeycomb systems [37–39]. In this region, the system dynamics is well described, in the continuum approximation, by the Dirac equation [37–39]. However, this equation becomes meaningless in the case of small finite fragments of honeycomb lattice because the band structure in these systems strongly differs from infinite honeycomb array [40,41].

Since we are interested in finding signatures of GF from classical light propagating in honeycomb PWA with cross sections of any size, we resort to a discrete description of the arrays instead of the usual continuum approximation [37–39].

To find these signatures in the nonlinear solutions of the system we follow a two-step protocol. First, since GF has been predicted as a lack of magnetic ordering in half-filled lattice graphene nanoflakes at zero energy [1], we set at the zero-energy-like state an infinite honeycomb PWA. For that purpose the phases associated with a Dirac point of the first Brillouin zone are imposed on the system. Second, since GF is an extensive phenomenon, we look for excitations in the form of extensive-field solutions in the presence of Kerr nonlinearity. We show that despite the fact that extensive

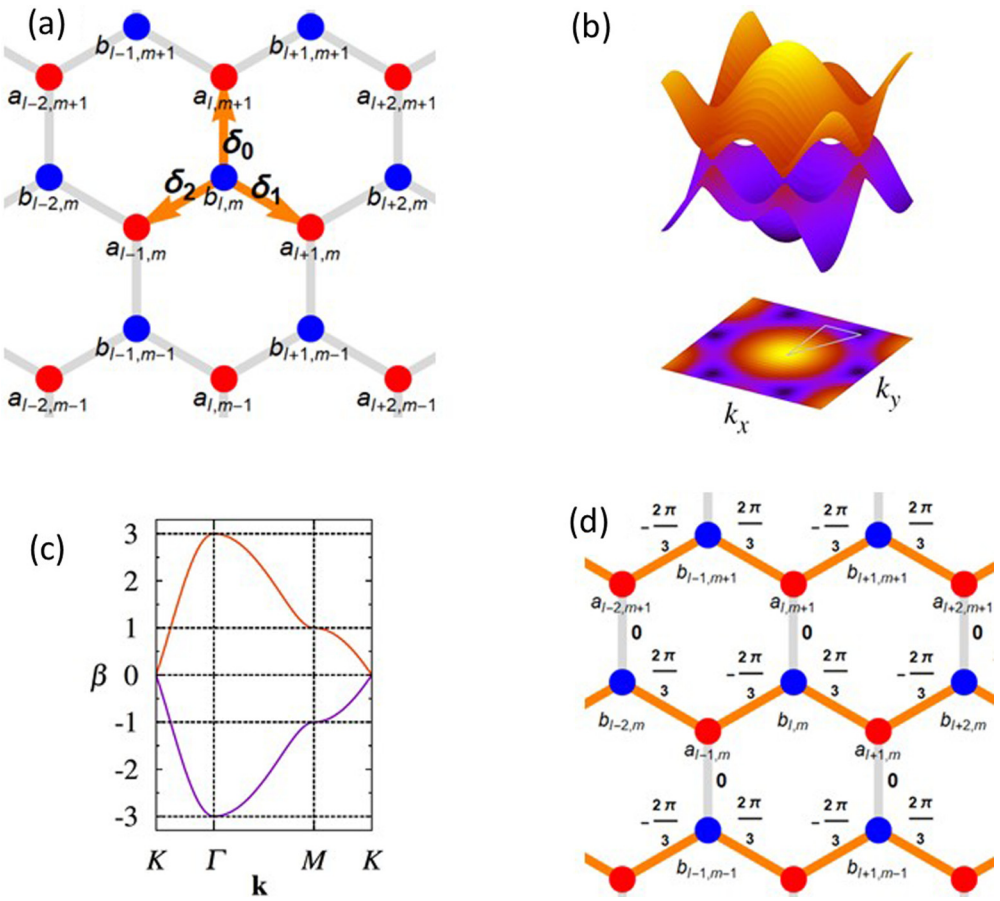

FIG. 1. (a) $\mathbf{N} = \{l, m\}$ site index distribution in the honeycomb lattice. $\boldsymbol{\delta}_j$ with $j = 0, 1, 2$ are displacement vectors between $a_{l',m'}$ and $b_{l,m}$ sites [39,42]. (b) The honeycomb band structure and its projection into the first Brillouin zone. (c) The honeycomb band structure along the symmetry points of the structure. (d) Configuration of negative (dark orange) and positive (light gray) couplings of the Honeycomb lattice at the Dirac point, $\mathbf{k} = (4\pi/(3\sqrt{3}), 0)$: The relative phases with respect to the b sites are also shown. All plotted quantities are dimensionless.

stationary collective excitations in infinite systems exist, they do not exist for finite fragments of the honeycomb lattice geometry. This behavior is due to the inherent frustrated nature of PWA with finite cross sections when configured in a Dirac point.

II. THEORY AND RESULTS

In the tight-binding approximation, the dynamics associated with the two lowest bands of the infinite nonlinear honeycomb PWA is well described by a discrete nonlinear Schrödinger equation (DNLSE) [23,29,39,42,43], reading as

$$i\,\partial_z \psi_{\mathbf{N}}(z) + C \sum_{\mathbf{N}' \neq \mathbf{N}} \psi_{\mathbf{N}'}(z) + U|\psi_{\mathbf{N}}(z)|^2 \psi_{\mathbf{N}}(z) = 0, \qquad (1)$$

where $\psi_{\mathbf{N}}$ is the complex electric field envelope function in the $\mathbf{N}$ waveguide. The index vector $\mathbf{N}'$ in Eq. (1) runs over nearest-neighboring waveguides; $C > 0$ is the coupling constant between waveguides, and U is the nonlinear coefficient of the cubic nonlinear response.

The DNLSE (1) not only describes the dynamics of honeycomb PWA [37,39,42] but also that of Bose-Einstein condensates (BECs) trapped in deep optical honeycomb lattices [38,39,42]. In the latter case the coordinate z in Eq. (1) is interpreted as time.

Here it is worth mentioning that the Kuramoto model [21,22,44] was suggested in Ref. [20] to study GF arising from disordered relative phases in discrete photonic systems. However, this model cannot be strictly derived from the linear approximation ($U = 0$) of Eq. (1). Therefore, the Kuramoto model is not appropriate for studying the physics of honeycomb PWA. For that reason, instead of studying GF emerging from disordered relative phases, here we study the amplitude behavior of classical laser beams propagating in PWA. In particular, we analyze the transverse wave propagation in the system as a collective excitation.

To proceed, we substitute a Floquet ansatz of the form $\psi_{\mathbf{N}} = \exp(i\beta z)\eta_{\mathbf{N}}$ into Eq. (1). Afterward, we use the Bloch ansatz, $\eta_{\mathbf{N}} = \exp(i\mathbf{k}\cdot\mathbf{r}_{\mathbf{N}})\phi_{\mathbf{N}}$, where $\mathbf{r}_{\mathbf{N}}$ is the transverse position of the $\mathbf{N}$ waveguide. Under these considerations, the stationary equation for the $\phi_{\mathbf{N}}$ functions reads as [42]

$$\beta\phi_{\mathbf{N}} = C \sum_{\mathbf{N}' \neq \mathbf{N}} \phi_{\mathbf{N}'} e^{i\mathbf{k}\cdot\Delta\mathbf{r}_{\mathbf{N}\mathbf{N}'}} + U|\phi_{\mathbf{N}}|^2\phi_{\mathbf{N}}, \qquad (2)$$

where $\Delta\mathbf{r}_{\mathbf{N}\mathbf{N}'} = \mathbf{r}_{\mathbf{N}'} - \mathbf{r}_{\mathbf{N}}$ denotes the displacement vectors between the $\mathbf{N}$ and $\mathbf{N}'$ waveguides [see Fig. 1(a)], so they connect the two honeycomb sublattices. In general $\Delta\mathbf{r}_{\mathbf{N}\mathbf{N}'} = \pm\boldsymbol{\delta}_j$, where $\boldsymbol{\delta}_j$ with $j = 0, 1, 2$ are plotted in Fig. 1(a). For simplicity we consider $|\boldsymbol{\delta}_j| = 1$.

In the absence of the Kerr nonlinearity ($U = 0$) the usual quasienergy band β can be obtained from Eq. (1) as a function of the Bloch wave vector $\mathbf{k}$ [see Fig. 1(b)] [37–39,42].

In half-filled graphene nanoflakes, GF has been predicted to emerge at the ground state, i.e., at the zero-energy eigenstate [1]. This suggests that in honeycomb PWA, GF may arise from configurations associated with zero-β collective excitations when $U = 0$ [linear case in Eq. (2)]. Notice that in infinite arrays, the level $\beta = 0$ intersects the Dirac points of the linear energy band [K points in Fig. 1(c)] [37–39]. So, in linear systems, the Bloch wave vector of a zero-β excitation should be chosen at one Dirac point.

In contrast to other physical setups exhibiting emergent GF [1–3,10–18,37], nonlinearity, in the form of the Kerr effect, is readily available in PWA [23,36]. In fact, little is known about the effect of nonlinearity on GF emergence in discrete systems. In general, the presence of nonlinearity increases the β-value accessible range of the system [42]. So, at the Dirac points we can expect similar behavior. It opens the possibility of looking for stationary solutions and its relation with emergent GF in unlikely and counterintuitive parameter regions such as the Dirac points.

In the following, since the experimental photonic setup allows us to impose the value of $\mathbf{k}$, for convenience we chose the Dirac point $\mathbf{k} = (4\pi/(3\sqrt{3}), 0)$. Extensive stationary solutions can be easily calculated by first assuming that $\phi_{\mathbf{N}}$ functions are real and second by distinguishing the fields of each sublattice [42], i.e., $\phi_{l,m+1} = a_{l,m+1}$ and $\phi_{l,m} = b_{l,m}$, where $m = 2n$ and $l \wedge n \in \mathbb{Z}$. Under these considerations Eq. (2) for $a_{l,m+1}$ and $b_{l,m}$ sites [see Fig. 1(a)] becomes

$$\beta\, a_{l,m+1} = \frac{C}{2}(2b_{l,m} - b_{l-1,m+1} - b_{l+1,m}) + U\, a_{l,m+1}^3 + i\,\frac{\sqrt{3}\,C}{2}(b_{l+1,m+1} - b_{l-1,m+1}), \tag{3}$$

and

$$\beta\, b_{l,m} = \frac{C}{2}(2a_{l,m+1} - a_{l-1,m} - a_{l+1,m}) + U\, b_{l,m}^3 + i\,\frac{\sqrt{3}\,C}{2}(a_{l+1,m} - a_{l-1,m}). \tag{4}$$

Since $a_{l,m+1}$ and $b_{l,m}$ are real functions, the constraints

$$a_{l+1,m} = a_{l-1,m} \quad \text{and} \quad b_{l+1,m+1} = b_{l-1,m+1} \tag{5}$$

should be imposed.

Interestingly, in this configuration the nearest neighboring (NN) sites with different l index are negatively coupled, while those NN sites with different m index are positively coupled [see Fig. 1(d)]. In addition, the relative-phase magnitude between NN negatively coupled sites is $\pm 2\pi/3$ and between positively NN coupled sites is zero.

The presence of negatively coupled sites has been identified as a necessary but not sufficient condition to observe GF emergence in network lattices [20,22,44,45]. So, to check the presence of GF signatures in PWA, we look for collective excitations in the form of a stationary solution of Eq. (3). In the case of spin lattices, GF has been associated with the inability to simultaneously pair all orbitals in the entire lattice [1]. In the same way, we associate the inability of the entire photonic array to bear spatially extensive stationary solutions with the GF emergence in nonlinear PWA systems.

Extensive solutions of Eqs. (3) and (4) can be determined by considering only constant fields, i.e., $a_{l,m+1} = A$ and $b_{l,m} = B$. In this case, it is straightforward to obtain algebraic expressions of the form

$$B = \pm A \quad \text{with} \quad A = \pm\sqrt{\beta/U}, \tag{6}$$

where $\beta\, U > 0$. Similar solutions can be found $\beta\, U < 0$ in the presence of a global phase $\pi/2$. Without loss of generality, in the following, we are going to consider only the case $\beta\, U > 0$.

The existence of A and B solutions, in Eq. (6), implies that at least for infinitely extended PWA, there exist stationary collective excitations that satisfy all constraints of the system. So, despite of the presence of negative couplings in the array, no GF signatures are observed in infinite systems. This result is counterintuitive, taking into account that in the literature only moving excitations, described by the 2D Dirac equations, have been reported in the vicinity of Dirac points in infinitely extended honeycomb systems [34,35,37–39,42,46].

Beyond unrealistic infinite systems, GF signatures have been observed in finite systems, for example, in honeycomb spin nanoflakes [1]. So, we may expect similar behavior in honeycomb PWAs with finite cross section. In fact, if we look at Eq. (3), it becomes apparent that the nontrivial solutions A and B, found in Eq. (6) for infinite systems, do not satisfy edge conditions if the honeycomb PWA has a finite cross section because the constraints that appear for real functions [see Eq. (5)] cannot be satisfied. This observation can be easily generalized to any nontrivial real extensive function $\phi_{\mathbf{N}}$. For example, since finite honeycomb PWAs have finite cross section, the site or sites with the highest l value, $l_{\max}$, are located at the edge. This implies that for $l > l_{\max}$ sites do not exist. So, at least one of the constraints in Eq. (5) cannot be satisfied by any nontrivial extensive field. This means that finite honeycomb PWAs, regardless of the cross-section shape, configured at a Dirac point unavoidably shows GF signatures.

Let us consider a laser beam propagating along a finite PWA with a rectangular cross section. A series of snapshots from numerical simulations of the transverse intensity distribution of the beam for four different propagation distances are shown in Fig. 2. The initial condition, plotted in Fig. 2(a), follows from Eq. (6) for the case $A = B = 1$ ($\beta = U = 1$). To follow the evolution of the beam, isointensity contour lines (contours that mark the same intensities) for the level values 0.96 and 1.01 are plotted in the figures. The region (plotted in white) between the two contour lines shows the evolution of the part of the beam with constant intensity ($\phi_{\mathbf{N}}^2 = 1$). We observe GF emergence as field distortions that appear at the array edges [see Figs. 2(b) and 2(c)] and move into the center. These distortions eventually destroy the initial stationary beam [white isointensity region between the two contour lines shown in Fig. 2]. So, in the long term, only moving excitations prevail in this configuration.

It is worth noting here that the constraints in Eq. (5) not only apply at the edges but also in the whole PWA cross section, regardless of the array shape. These constraints can be satisfied only by extensive fields. So, there does not exist any localized field (with finite energy) that can remain stationary in a honeycomb PWA configured at a Dirac point. This

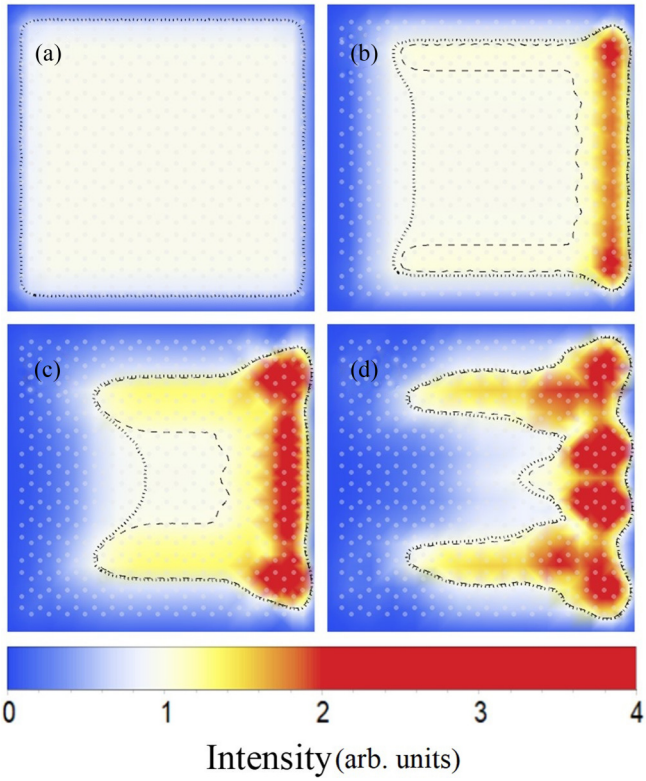

FIG. 2. Snapshots of the transverse intensity distribution, $|\psi_N|^2$, at $z = 0$ (a), $z = 2.0$ (b), $z = 4.0$ (c), and $z = 6.0$ (d) of a PWA with a rectangular cross section and configured at a Dirac point. At $z = 0$ the initial condition follows from Eq. (6) with $A = B = 1$ ($\beta = U = 1$). In the color scale, white corresponds to values near unity. On the other hand, red colors correspond to any values above 2. The dotted and dashed contour lines are isointensity lines (contours that mark the same intensities) for the level values 0.96 and 1.01, respectively.

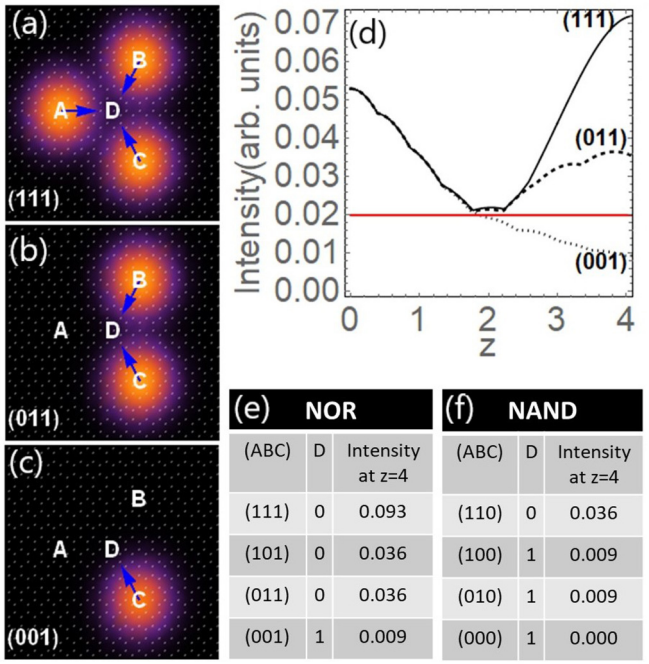

(e) NOR

(ABC)	D	Intensity at z=4
(111)	0	0.093
(101)	0	0.036
(011)	0	0.036
(001)	1	0.009

(f) NAND

(ABC)	D	Intensity at z=4
(110)	0	0.036
(100)	1	0.009
(010)	1	0.009
(000)	1	0.000

FIG. 3. Intensity distribution of three (a), two (b), or one (c) Gaussian laser beams in a equilateral triangular configuration. (d) Evolution of the peak intensity along the dimensionless propagation coordinate z. Truth tables of NOR (e) and NAND (f) gates.

nonexistence of stationary localized fields is also a signature of the inherent frustration of the array configuration.

The fact that GF is unavoidable in finite honeycomb PWA (regardless of the array cross-section shape) configured in a Dirac point is an interesting insight, because in spin lattices the absence of frustration (observed as perfect pairing of all orbitals) has been predicted in some particular graphene nanoflake shapes [1]. This difference in the behavior between spin lattices and PWA systems hints at the possibility of constructing logic gates with finite PWA systems, in the spirit of spintronic devices [1], without the burden of designing special geometric shapes for the honeycomb array.

For example, with a simple honeycomb PWA with a rectangular cross section [see Figs. 3(a)–3(c)] we can easily mimic the NOR and NAND gates proposed in Ref. [1] for spin-lattice systems. For that purpose we consider finite energy excitations in the form of Gaussian laser beams propagating along the array. Figure 3(d) shows the peak-maximum-intensity behavior of three, or less, input laser beams propagating along the propagation coordinate z of a rectangular shape of 561 photonic evanescently coupled waveguides. A single beam in the system can be interpreted as a logic one, otherwise the absence implies a logic zero. The beams are placed to form an equilateral triangle in the array cross section [see Figs. 3(a)–3(c), regions A, B, and C]. The beam Bloch wave vector of each Gaussian beam is chosen to be one of the six Dirac points of the band structure, such that each beam transversely moves across the geometrical center of the triangle [region D in Figs. 3(a)–3(c)]. The initial amplitude and envelope shapes are the same for any beam, so the initial peak-maximum-intensity ($z = 0$) remains the same if one or more beams are propagating in the PWA system. Depending on the number of beams initially launched, the maximum intensity of the system can reach different values when the beams cross each other and superimpose in region D, which corresponds to the propagation distance $z = 4$. To define the NOR and NAND operation from the three beams, we consider that two of them behave as information bits and the remaining one programs the setup to be NOR or NAND gate [1], as shown in Figs. 3(e) and 3(f). In the regions A, B, and C, the presence (absence) of a beam corresponds to a logic one (zero). In the region D we impose a threshold [red line in Fig. 3(d)]. A maximum intensity in the region D (at $z = 4$) below (above) the threshold corresponds to a logic one (zero). With this simple setup the NOR and NAND operations can be performed.

To get further insight into the emergence of GF in optical system, we next focus with more detail on the sign of the coupling constant C. In this regard, in the case of thousands of coupled lasers in Ref. [20] it has been suggested that negative coupling constants are more appropriate than the positive ones to observe GF signatures. This is because negatively coupled spin lattices have been shown to be prone to large degeneracy, independently of the Hamiltonian symmetry. On the other hand, by using the Kuramoto model, it has been argued that GF signatures emerge under the simultaneous presence of positive and negative coupling constants in the system [44]. In the case

of coupled waveguide arrays, the coupling constant between NN guides in Eq. (1) is by definition positive. However, as discussed before, depending on the value of $\mathbf{k}$, we can effectively change the sign in front of the couplings. For instance, we have shown that at the Dirac points there are one positive and four negative couplings in each unit cell [see Fig. 1(d)]. So, the fact that most of the couplings, but not all, are negative agrees well with GF emergence observed here and in other frustrated systems [20,44].

To verify whether the proportion between positive and negative couplings is a determining factor in the emergence of GF, we revisit a case where the number of positive couplings is higher than negatives in PWA systems. This can be easily achieved by configuring the array system in one of the M points of the band structure [see Fig. 1(c)]. For that purpose we impose $\mathbf{k} = (0, 2\pi/3)$ into Eq. (2) and assume the functions $\phi_{\mathbf{N}}$ to be real. Here we also distinguish the fields of each sublattice, as it was done for Eqs. (3) and (4). So, we obtain that

$$\beta a_{l,m+1} = C(b_{l-1,m+1} + b_{l+1,m+1} - b_{l,m}) + U a^3_{l,m+1} \quad (7)$$

and

$$\beta\, b_{l,m} = C(a_{l-1,m} + a_{l+1,m} - a_{l,m+1}) + U\, b^3_{l,m}. \quad (8)$$

Interestingly, Eqs. (7) and (8) do not contain any imaginary term. So, in contrast to Eqs. (3) and (4), in the present case no additional constraints are needed to obtain real solutions. Moreover, in this system configuration, there are one negative and four positive couplings in each unit cell. In fact, the configuration is similar to that shown in Fig. 1(d), but with signs of the couplings flipped.

In Fig. 4, we compare the behavior of the quasienergy β along a honeycomb PWA for collective excitations at the Dirac (red dashed line) and M (black continuous line) points. In both cases a rectangular cross-section shape of the array, similar to that shown in Fig. 2, is considered and the parameter values $\beta = U = 1$ are imposed. The initial excitation in the M point has been calculated using the imaginary propagation method, as described in Ref. [42]. In this case, the initial constant behavior of β shows that the initial solution is stationary. Eventually ($z > 6$ in Fig. 4) it is distorted by instabilities [42]. The fact that an initial stationary solution can be computed means that Eq. (7) is fully satisfied, so no GF signatures can be observed here. On the other hand, at the Dirac point, we consider as an initial condition the solution given in Eq. (6). Notice that the computed β value at $z = 0$, in Fig. 4, is slightly different from the value of unity. This

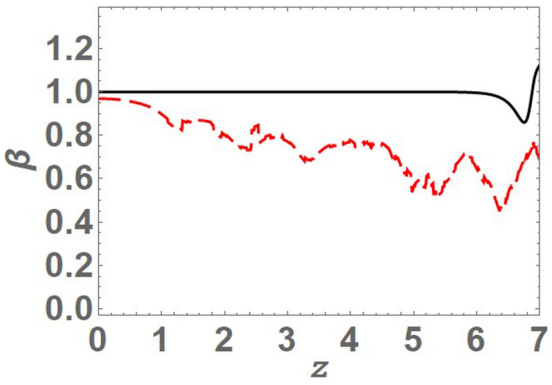

FIG. 4. Evolution of the quasienergy β of extensive fields at the Dirac point (dashed line) and the M point (solid line) of the Band structure. $\beta = 1$ at $z = 0$. β and z are dimensionless.

slight discrepancy follows from the fact that the solution in Eq. (6) does not satisfy the edge conditions of finite arrays. As expected, in Fig. 4, we observe that the initial solution at the Dirac point never reaches a stationary state due to the inherent GF of the configuration. These results further confirm that the sign distribution of the couplings is important for the GF emergence in honeycomb PWA systems and agree with behavior observed in magnetically frustrated systems.

III. SUMMARY AND CONCLUSIONS

In summary, we have shown that classical light propagating in honeycomb photonic waveguide arrays with finite cross section exhibits signatures of geometrical frustration. Although the physics as well as dimensions and energies of frustrated spin lattices are different from those of photonic waveguides arrays, we have observed that both systems can exhibit similar behavior when geometrical frustration is present. This opens new avenues for studying frustration in lattice geometries beyond what is achievable with magnetically frustrated systems.

ACKNOWLEDGMENTS

This work was supported in part by the Fondo Nacional de Desarrollo Científico y Tecnológico (FONDECYT) Projects No. 1150612 and No. 1141223, and by the Programa Iniciativa Científica Milenio (ICM) Grant No. 130001.

[1] W. L. Wang, O. V. Yazyev, S. Meng, and E. Kaxiras, Phys. Rev. Lett. **102**, 157201 (2009).
[2] J. W. F. Venderbos, M. Daghofer, J. van den Brink, and S. Kumar, Phys. Rev. Lett. **107**, 076405 (2011)
[3] R. Kaneko, L. F. Tocchio, R. Valenti, and C. Gros, Phys. Rev. B **94**, 195111 (2016).
[4] T. Neupert, L. Santos, C. Chamon, and C. Mudry, Phys. Rev. Lett. **106**, 236804 (2011).
[5] E. Tang, J.-W. Mei, and X.-G. Wen, Phys. Rev. Lett. **106**, 236802 (2011).
[6] M. Hirschberger, J. W. Krizan, R. J. Cava, and N. P. Ong, Science **348**, 106 (2015).
[7] A. Sapkota, B. G. Ueland, V. K. Anand, N. S. Sangeetha, D. L. Abernathy, M. B. Stone, J. L. Niedziela, D. C. Johnston, A. Kreyssig, A. I. Goldman, and R. J. McQueeney, Phys. Rev. Lett. **119**, 147201 (2017).
[8] D. J. P. Morris, D. A. Tennant, S. A. Grigera, B. Klemke, C. Castelnovo, R. Moessner, C. Czternasty, M. Meissner, K. C. Rule, J.-U. Hoffmann, K. Kiefer, S. Gerischer, D. Slobinsky, and R. S. Perry, Science **326**, 411 (2009).

[9] C. Nisoli, R. Moessner, and P. Schiffer, Rev. Mod. Phys. **85**, 1473 (2013).
[10] J. Simon, W. S. Bakr, R. Ma, M. E. Tai, P. M. Preiss, and M. Greiner, Nature (London) **472**, 307 (2011).
[11] J. Struck, C. Olschlager, R. Le Targat, P. Soltan-Panahi, A. Eckardt, M. Lewenstein, P. Windpassinger, and K. Sengstock, Science **333**, 996 (2011).
[12] J. W. Britton, B. C. Sawyer, A. C. Keith, C.-C. J. Wang, J. K. Freericks, H. Uys, M. J. Biercuk, and J. J. Bollinger, Nature (London) **484**, 489 (2012).
[13] M. Sigrist and T. M. Rice, Rev. Mod. Phys. **67**, 503 (1995).
[14] M. V. Feigel'man, L. B. Ioffe, V. B. Geshkenbein, P. Dayal, and G. Blatter, Phys. Rev. B **70**, 224524 (2004).
[15] R. F. Wang, C. Nisoli, R. S. Freitas, J. Li, W. McConville, B. J. Cooley, M. S. Lund, N. Samarth, C. Leighton, V. H. Crespi, and P. Schiffer, Nature (London) **439**, 303 (2006).
[16] Y. Han, Y. Shokef, A. M. Alsayed, P. Yunker, T. C. Lubensky, and A. G. Yodh, Nature (London) **456**, 898 (2008).
[17] P. Tierno, Phys. Rev. Lett. **116**, 038303 (2016).
[18] A.W. Glaetzle, M. Dalmonte, R. Nath, C. Gross, I. Bloch, and P. Zoller, Phys. Rev. Lett. **114**, 173002 (2015).
[19] M. Biondi, E. P. L. van Nieuwenburg, G. Blatter, S. D. Huber, and S. Schmidt, Phys. Rev. Lett. **115**, 143601 (2015).
[20] M. Nixon, E. Ronen, A. A. Friesem, and N. Davidson, Phys. Rev. Lett. **110**, 184102 (2013).
[21] S. N. Dorogovtsev, A. V. Goltsev, and J. F. F. Mendes, Rev. Mod. Phys. **80**, 1275 (2008).
[22] Z. Levnajic, Phys. Rev. E **84**, 016231 (2011).
[23] F. Lederer, G. I. Stegeman, D. N. Christodoulides, G. Assanto, M. Segev, and Y. Silberberg, Phys. Rep. **463**, 1 (2008).
[24] H. Trompeter, W. Krolikowski, D. N. Neshev, A. S. Desyatnikov, A. A. Sukhorukov, Y. S. Kivshar, T. Pertsch, U. Peschel, and F. Lederer, Phys. Rev. Lett. **96**, 053903 (2006).
[25] V. S. Shchesnovich, A. S. Desyatnikov, and Y. S. Kivshar, Opt. Express **16**, 14076 (2008).
[26] E. Arévalo and L. Morales-Molina, Europhys. Lett. **96**, 60011 (2011).
[27] O. Bahat-Treidel, O. Peleg, M. Grobman, N. Shapira, M. Segev, and T. Pereg-Barnea, Phys. Rev. Lett. **104**, 063901 (2010).
[28] T. Schwartz, G. Bartal, S. Fishman, and M. Segev, Nature **446**, 52 (2007).
[29] M. C. Rechtsman, J. M. Zeuner, A. Tünnermann, S. Nolte, M. Segev, and A. Szameit, Nat. Photon. **7**, 153 (2013).
[30] F. D. M. Haldane and S. Raghu, Phys. Rev. Lett. **100**, 013904 (2008).
[31] M. C. Rechtsman, Y. Plotnik, J. M. Zeuner, D. Song, Z. Chen, A. Szameit, and M. Segev, Phys. Rev. Lett. **111**, 103901 (2013).
[32] M. C. Rechtsman, J. M. Zeuner, Y. Plotnik, Y. Lumer, D. Podolsky, F. Dreisow, S. Nolte, M. Segev, and A. Szameit, Nature **496**, 196 (2013).
[33] O. Zilberberg, S. Huang, J. Guglielmon, M. Wang, K. P. Chen, Y. E. Kraus, and M. C. Rechtsman, Nature **553**, 59 (2018).
[34] A. K. Geim and K. S. Novoselov, Nat. Mater. **6**, 183 (2007).
[35] A. H. Castro Neto, F. Guinea, N. M. R. Peres, K. S. Novoselov, and A. K. Geim, Rev. Mod. Phys. **81**, 109 (2009).
[36] M. Polini, F. Guinea, M. Lewenstein, H. C. Manoharan, and V. Pellegrini, Nat. Nanotechnol. **8**, 625 (2013)
[37] M. J. Ablowitz, S. D. Nixon, and Y. Zhu, Phys. Rev. A **79**, 053830 (2009).
[38] L. Haddad and L. Carr, Physica D: Nonlinear Phenomena **238**, 1413 (2009).
[39] E. Arévalo and L. Morales-Molina, Phys. Rev. A **93**, 053816 (2016).
[40] Y.-W. Son, M. L. Cohen, and S. G. Louie, Phys. Rev. Lett. **97**, 216803 (2006).
[41] M. Y. Han, B. Ozyilmaz, Y. Zhang, and P. Kim, Phys. Rev. Lett. **98**, 206805 (2007).
[42] E. Arévalo and C. Mejia-Cortes, Phys. Rev. A **90**, 023835 (2014).
[43] M. I. Molina and Y. S. Kivshar, Opt. Lett. **35**, 2895 (2010).
[44] J. A. Acebron, L. L. Bonilla, C. J. P. Vicente, F. Ritort, and R. Spigler, Rev. Mod. Phys. **77**, 137 (2005).
[45] D. H. Zanette, Europhys. Lett. **72**, 190 (2005).
[46] O. Peleg, G. Bartal, B. Freedman, O. Manela, M. Segev, and D. N. Christodoulides, Phys. Rev. Lett. **98**, 103901 (2007).